Composites Part B 176 (2019) 107299

Contents lists available at ScienceDirect

Composites Part B

journal homepage: www.elsevier.com/locate/compositesb

Multi-walled carbon nanotube and carbon nanofiber/ polyacrylonitrile aerogel scaffolds for enhanced epoxy resins

Akram Dourani [a,b,*], Majid Haghgoo [a], Masood Hamadanian [b]

[a] Space Transportation Research Institute, Iranian Space Research Center, Tehran, Iran
[b] Institute of Nano Science and Nano Technology, University of Kashan, Kashan, Iran

ARTICLE INFO

Keywords:
Aerogel
Multi–walled carbon nanotube
Polyacrylonitrile
Infiltration
Percolation threshold

ABSTRACT

Despite the unique characteristics of carbon nanostructures such as carbon nanotube (CNTs) and carbon nanofibers (CNFs), their practical applications are limited because of their extremely low solubility and poor dispersion characteristics. To obtain composites with favorable electrical, thermal and mechanical properties, a network of nanofiller/polyacrylonitrile (PAN) aerogel was prepared by non-solvent and thermally induced phase separation (NIPS/TIPS) method and used as a scaffold to create epoxy nanocomposite. Compared with the conventional mixing, this method brought about a considerable increase of compressive strength (about 500%). Furthermore, an electrical percolation threshold as low as 0.0028 and 0.019 vol % was observed for CNT/polyacrylonitrile/epoxy nanocomposites (CNT/PA/E) and CNF/polyacrylonitrile/epoxy nanocomposites (CNF/PA/E), respectively. To the best of our knowledge, this small amount of percolation threshold has not yet been reported for CNT and CNF based nanocomposites. Such intriguing performance can mainly be related to a three-dimensional nanotube and nanofiber network structure in the resin matrix.

1. Introduction

Epoxy resins are important type of thermosetting polymers which, due to their unique physical, mechanical and chemical resistance are widely used in protective coatings, adhesives, high performance composites, molding and electrical applications [1,2] . Despite these outstanding properties, cured epoxy resin is fragile and has a low impact resistance. Therefore, in order to solve this problem, the nanofillers as a reinforcement component are introduced in the epoxy matrix [3]. Among nanofillers, carbon nanotubes (CNTs) have been considered for a variety of promising intrinsic properties such as unique electrical [4]and thermal [5]properties and high strength-to-weight ratio [6,7]. Nonetheless, the major limitation for CNT applications is the poor dispersion of the nanotubes in common solvents and polymer matrices, due to the tendency of the nanotubes to be in the form of clusters and bundles [8]. Several techniques have been used for the homogeneous distribution of CNTs in epoxy such as high speed shear mixing, sonication and functionalization such as amine and silane modification [9,10]. However, these methods diminish intrinsic properties of nanotubes by reducing their effective aspect ratio, so that the mechanical properties of CNTs are often well below the theoretical estimates. Recently, the methods based on backfilling porous structures from nanotubes such as fibers, sponges and buckypaper have been reported. These methods are often include chemical vapor deposition that contains impurities produced during synthesis process [11,12] An attractive alternative can be the use of lightweight, three-dimensional porous network of CNT template filled with resin. Among the porous materials based on carbon nanotubes, CNT aerogels have been attracted a lot of attention due to interesting features such as high strength-to-weight, high surface area and tremendous thermal and electrical conductivity [13,14].

Recently, reports have been published on the preparation of elastic materials based on CNT aerogels. The CNT/poly dimethysiloxane (PDMS) composite aerogels were made using the infiltrating of PDMS into a CNT aerogel sample by Worsley et al. [14]. The electrical conductivity of the final composite reached more than 1 S cm^{-1} and its elastic modulus showed an increase of 300% with 1 vol % nanotube. In another work, they [15] have fabricated novel metal oxide/CNT nanocomposite using the coating of a metal oxide layer on the surface of single walled CNT/carbon (SWCNT/C) aerogel support. The formation of CNT/metal oxide aerogel composite was carried out through infiltration and deposition of the oxides without degradation of the CNT support. Cao et al. [16] were able to make epoxy nanocomposite based

* Corresponding author. Space Transportation Research Institute, Iranian Space Research Center, Tehran, Iran.
E-mail address: a.dourani@isrc.ac.ir (A. Dourani).

https://doi.org/10.1016/j.compositesb.2019.107299
Received 4 February 2019; Received in revised form 29 July 2019; Accepted 11 August 2019
Available online 13 August 2019
1359-8368/

on CNT sponge using direct injection of resin to the CNT scaffold. The resulting composite had electrical resistivity of 10–30 Ω cm which was much less than the amount obtained by composites prepared by conventional mixing method. Zhao [17]and coworkers have proposed an infiltration−evaporation−curing method in order to uniform coating of polymers on the wall of graphene aerogel and forming PDMS/graphene aerogel composite. Recently, in a similar work, Kyo et al. [18] prepared GA/epoxy nanocomposites by infiltrating method . The results showed a considerable value of conductivity (2×10^{-3} S/cm) with 0.25 wt % of GA and an enhancement of 64% in fracture toughness with 1.4 wt % graphene.

We recently reported a new synthesis route to prepare lightweight carbon nanostructure based on CNT aerogel monoliths with exceptional electrical, thermal and mechanical properties [19,20]. Non-solvent and thermally induced phase separation (NIPS/TIPS) procedure was used to compose the aerogels. Because of these unique characteristics, these ultra-light, robust aerogels could allow the formation of novel multifunctional CNT nanocomposites.

We publish here an infiltration procedure to construct epoxy nanocomposites with polyacrylonitrile/multi-walled carbon nanotubes and polyacrylonitrile/carbon nanofiber aerogels scaffold. The thermal and electrical conductivity of the nanocomposites were measured and the experimental results were compared with the corresponding theories. In addition, the mechanical properties of these aerogel nanocomposite were evaluated and the obtained results were compared with the results of the other research works on CNT and CNF/epoxy nanocomposite.

2. Experimental section

2.1. Materials

Polyacrylonitrile (PAN) powder (Sigma-Aldrich), DMF (N, *N*-dimethyl formamide, Merck), Acetone (Merck), functional multi-walled carbon nanotubes (COOH content: 2.6%, length: 5.8 μm, outer diameter: 8–15 nm and number of walls: 3–12, PlasmaChem), Carbon nanofiber (length:5–50 μm, outer diameter: 200–400 nm and purity >95 wt %, Neutrino), epoxy resin (EPON™ Resin 828, Hexion), polyetheramine (JEFFAMINE® D-400, Huntsman) were used as received.

2.2. Preparation of epoxy infiltrated MWCNT/PAN and CNF/PAN aerogel nanocomposites

The CNT/PA aerogels with a MWCNT loading of 0–25 wt % and a monolith density of 50–500 mg cm^{-3} were produced in a manner previously reported [19]. The synthesis process of CNF/PA samples was performed similar to the CNT/PA ones. For preparation of aerogel nanocomposite, the curing agent was first added to the epoxy resin and the solution was mixed monotony with weight mix ratio 50:31(epoxy: curing agent), according to the manufacturer's brochure. Then the CNT aerogel monolith was fully floated in the resin for 15 min. Then to complete the infiltration process, degassing was performed under vacuum.

Finally, the infiltrated CNT/PA was cured at 60 °C to make the nanocomposite. In order to produce carbonized samples, organic composites were pyrolyzed at 850 °C for 6 h in N_2 atmosphere.

2.3. Preparation of MWCNT and CNF/epoxy nanocomposites by simple mixing

As for the preparation of MWCNT/epoxy nanocomposite, first, carboxylated CNTs were dispersed in acetone, under sonication for 30 min. Then, the dispersion with 0-25 wt% CNT were added to the epoxy resin. Then mixture dispersed for 1 h using an ultrasonic homogenizer at 80 °C following by degassing under vacuum condition at 60 °C for 24 h. Afterwards, by adding harder to the samples, the curing was performed under magnetic stirring at room temperature. The synthesis of CNF/epoxy nanocomposites was performed in a similar route. All samples are named according to Table 1.

2.4. Physical characterization

The linear shrinkage of the samples was calculated with respect to their dimensional change before and after drying. The bulk density (ρ_b) was obtained according to the weight and volume of the pure aerogels or composites. The porosity (ε) was calculated as $\varepsilon = \left(1 - \frac{\rho_b}{\rho_s}\right) \times 100$, Where ρ_s is the skeletal density which is equal to 2.1, 2, 1.18, 2.62 and 1.16 g/cm^3 for MWCNT,CNF, PAN, CA and epoxy respectively. The field emission scanning electron microscopy (FESEM, TESCAN LYRA3 apparatus) was used to observe the microstructure of the samples. For this purpose, the specimens were first broken down in liquid nitrogen and then coated with Au/Pd. Evaluation of the dispersion state of nanotubes and nanofibers was performed by the transmission electron microscopy (TEM, LIBRA 200 MC,Carl Zeiss SMT, Germany, 200 kV) . In order to prepare samples, MWCNT was dispersed in DMF via sonication for 30 min and diluted at a ratio of 1–60.

The compressive strength of cylindrical samples was measured using a universal testing machine (Hegewald & Peschke, Inspekt 50, Germany). A 50 kN load cell was employed with a rate of 2.5 mm/min. The specific heat capacity (C_p) of the samples was measured by differential scanning calorimetry (DSC) thermal analysis using a PT10 Platinum series (Linseis). Most of the measurements were collected over a temperature range of 0–300 °C at a heating rate of 2.5 °C/min. The TGA analysis of the samples was performed under air atmosphere at a rate of 2.5 °C/min, up to 800 °C using a PT-1600 (Linseis). Using Xenon Flash Thermal Constant Analyzer (XFA 500, Linseis) can be obtained thermal diffusion coefficient. According to the thermal diffusion coefficient measurements and using the following equation, the total effective thermal conductivity, k_{eff} of the samples was obtained [21]:

$$k_{eff} = \alpha(T)\, \rho\, C_p(T) \quad (1)$$

Table 1
Composition of the starting dispersions and the final composites.

Sample code[a]	$C_{MWCNT(CNF)\text{-}mix}$ (W/V)[b]	Ø[c]
CNT/PA/E000	0.0000	0.00
CNT/PA/E001	0.0002	0.01
CNT/PA/E010	0.0017	0.10
CNT/PA/E050	0.0085	0.50
CNT/PA/E100	0.0170	1.00
CNT/PA/E165	0.2805	16.5
CNF/PA/E000	0.0000	0.00
CNF/PA/E001	0.0002	0.01
CNF/PA/E010	0.0016	0.10
CNF/PA/E050	0.0084	0.50
CNF/PA/E100	0.0169	1.00
CNF/PA/E165	0.2789	16.5
CNT/E000	0.0000	0.00
CNT/E001	0.0002	0.01
CNT/E010	0.0019	0.10
CNT/E050	0.0089	0.50
CNT/E100	0.0177	1.00
CNT/E165	0.3211	16.5
CNF/E000	0.0000	0.00
CNF/E001	0.0002	0.01
CNF/E010	0.0018	0.10
CNF/E050	0.0092	0.50
CNF/E100	0.0183	1.00
CNF/E165	0.3585	16.5

[a] In the sample codes, CNT, CNF, PA and E stand for carbon nanotube, carbon nanofiber, polyacrylonitrile and epoxy, respectively. The amount of PAN was kept constant in all formulations and chosen equal to 4 wt %. After pyrolysis PA is replaced with CA.
[b] Weight percentage of MWCNT or CNF in the primary mixture.
[c] Total volume fraction of MWCNT or CNF in the final composite.

Multiple thermal diffusivity (α) and specific heat capacity (C_p) measurements were made at room temperature.

3. Results and discussion

3.1. Microstructure and morphology of aerogel nanocomposites

In the present work, the MWCNT/PAN aerogel was used as a template in which the resin infiltrated into its pores. A schematic of synthesis method is shown in Fig. 1a and the optical image of pure and composite samples before and after infiltration was showed in Fig. 1b. The TEM images of the samples containing 0.01 v/v% CNT and CNF are shown in are shown in Fig. 2. The images showed that approximately most CNTs and CNFs were disentangled and isolated. It could be estimated that the length of the CNTs and CNFs were decreased to about 1–5 μm and 5–20 μm, and the diameter of CNTs and CNFs were typically in the range of 8–15 nm and 100–400 nm, respectively. Therefore, one can conclude that despite the separation of nanotubes and nanofibers from each other, their longitudinal fracture has not occurred during sonication.

The microstructure of the CNT and CNF aerogels before and after infiltration with typical nanofiller loading of 0.1 v/v% was appraised using SEM (Fig. 3). Fig. 3a shows the formation of an interconnected structure of nanotubes within the highly porous polymer matrix without observing the aggregation of the nanotubes in the aerogel composite, indicating that MWCNTs dispersed uniformly in the PAN composite gel precursor. After epoxy infiltration (Fig. 2b), one can observe that most of the aerogel pores is filled with epoxy. Fig. 3c shows SEM image of the CNT/EN sample. The presence of pulled-out nanotubes at the fracture surface of the composite indicates the weak links in the interface between the nanotube and the resin. While, the fractured surface of the MWCNT aerogel composites is quite different (Fig. 3b). The surface looks much denser and only a number of nanotubes can be seen as dots which are ruptured at the failure surface. SEM image of a typical CNF aerogel is shown in Fig. 3d. The observations indicate that the nanofibers are highly interconnected with large number of junctions and form a relatively uniform cellular structure with a wide range of particle size from nano to micro. The microstructure of the CNF aerogel exhibited an interconnected sponge-like porous texture with hierarchical structure; i.e., diffused area with less aerogel density that make open micrometric channels. Fig. 3e–f shows SEM images of nanofiber/epoxy resin nanocomposites containing 0.1 v % CNF. The SEM image of CNF/PA-filled resin is illustrated in Fig. 3e and CNF/E nanocomposite can be seen in Fig. 3f. The results show that nanofibers are uniformly

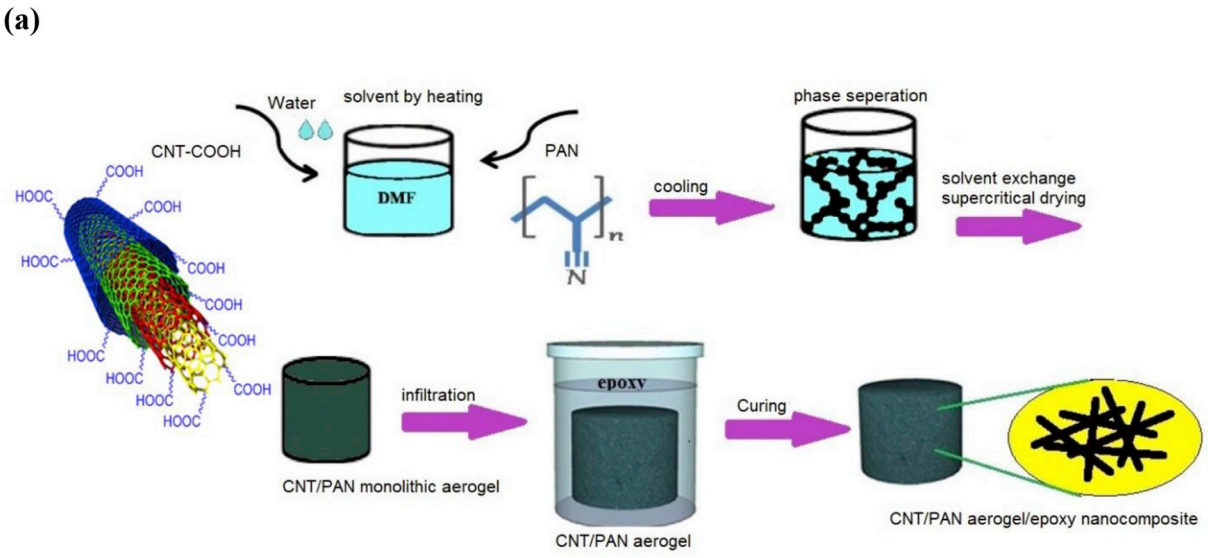

Fig. 1. (a) A schematic of the synthesis method, (b) The monoliths of (i) CNT/PA (ii) CNT/PA/E (iii)PA and (iv) PA/E.

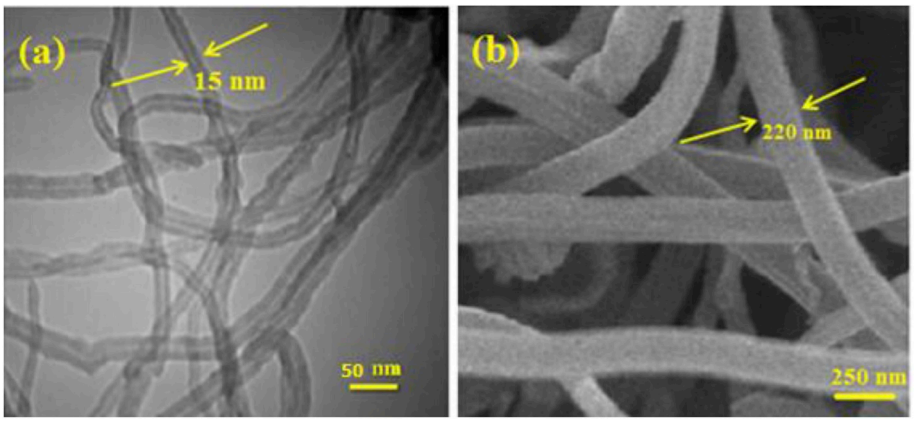

Fig. 2. Typical TEM image of a MWCNT (a) and CNF (b) suspension.

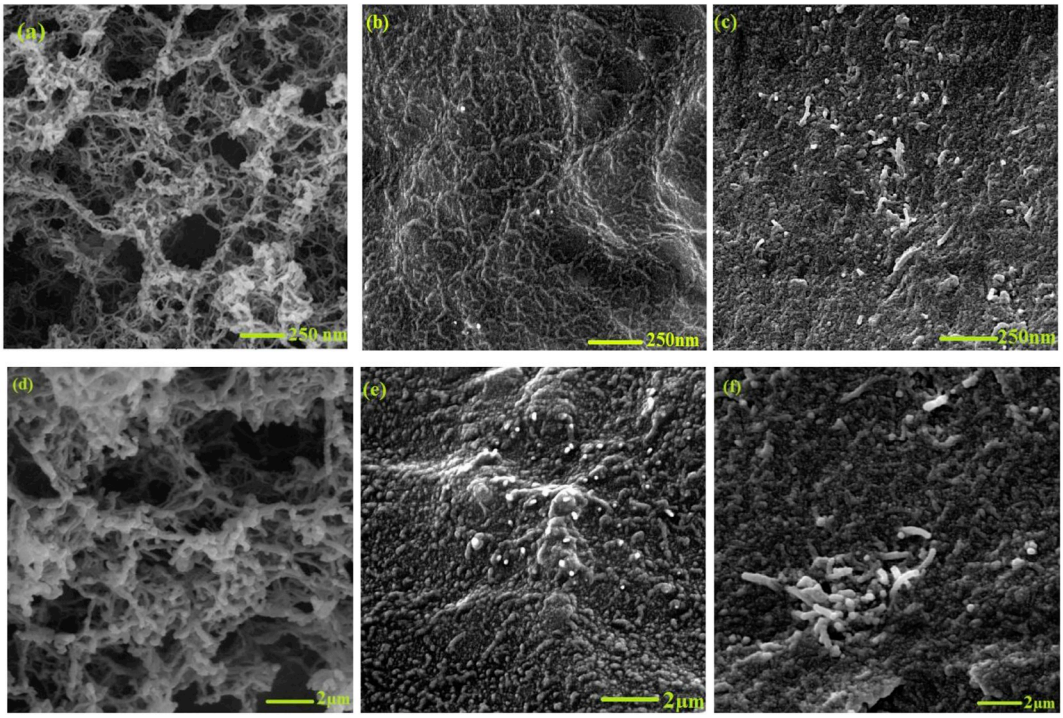

Fig. 3. SEM images of (a) CNT/PA, (b) CNT/PA/EN, (c) CNT/E, (d) CNF/PA, (e)CNF/PA/E and (f)CNF/E containing 0.1%v nanofiller.

distributed in the polymer matrix in both samples. As shown in Fig. 3e, some of the CNFs were pulled out of the epoxy matrix, but their number was relatively limited compared to ones embedded in the matrix (Fig. 3f) which suggests a good interfacial adhesion. The porous properties of CNT/PA and CNF/PA and aerogel epoxy nanocomposite with 0.1% v nanofiller are compared in Table 2. The obtained results revealed that the porous properties of the three samples were almost similar. This indicates that adding nanofiller (at least 0.1% v) had no significant effect on the density, shrinkage and porosity and also these parameters were not dependent on the nanofiller type.

The obtained results showed that the porosity of the nanocomposites reached less than 1% after infiltration by the resin. This is in good agreement with the SEM observations. Microscopic images indicate that the pore of aerogels was fully occupied with the near resin and the size of the epoxy blocks in void space between aerogel network is about 1–2 μm which is in accordance with the size of the pores in the aerogel, indicating the structure of the aerogel network and uniformity of nanocomposite is preserved well after infiltrating with resin.

The efficacy of CNT concentration level on the samples density of the

Table 2
The porous properties of CNT (CNF)/PA and epoxy composite.

Sample code	ρ (g/cm^3) ±0.01	$\%\Delta L/L$[a] ±0.01	D_{ave}[b] (μm) ±0.01	V_{total}[c] (cm^3/gr) ±0.02	ε[d] % ±0.02
PA	0.06	5.00	2.01	14.31	94.31
CNT/PA 010	0.06	4.87	1.78	15.01	94.52
CNF/PA 010	0.06	4.98	1.90	14.76	94.40
CNT/PA 010/E	1.15	–	–	0.21	0.53
CNF/PA010/E	1.07	–	–	0.28	0.70

[a] The linear shrinkage.
[b] Average pore diameter obtained from mercury porosimetry.
[c] Pore volume estimated from $V_{total} = .^1/_{\rho_b} - {}^1/_{\rho_s}$
[d] Porosity percent estimated from $\varepsilon = (1 - \rho_b/\rho_s) \times 100$.

pure and epoxy infiltrated CNT aerogels before and after pyrolysis is illustrated in Fig. 4. As reported in our previous work [20], the density and the linear shrinkage decrease with the CNT content increase. This was related to the higher mechanical strength of the CNT contained composites compared to that of pure ones. This can preserve the sample's dimension to some extent, when capillary forces are applied during drying process. After infiltration with epoxy resin, a reverse trend is observed: with increasing nanotube content, the samples density is increased. A plausible explanation can be corresponding to the existence of higher proportion of macropores in the porous texture of the samples with higher concentration of CNT [19]. The viscose resin could insert the larger voids more easily, so that it is more probable that all pores are occupied with the resin in the case of the samples with higher pore size.

3.2. Electrical properties of aerogel nanocomposites

The electrical conductivity of the CNT/CA/E and CNF/CA/E composites with different nanofiller concentration is plotted in Fig. 5. The σ_{eff} and σ_m were defined as the electrical conductivity of the epoxy infiltrated carbonized PAN with and without CNT, respectively. Comparing the conductivity of the epoxy composites in this work and the CNT/CA results of our previous work [21] revealed that the electrical conductivity of the CNT aerogel was preserved in the insulating matrices. No change in the conductivity indicates that the conductive scaffold is intact. As reported by Haghgoo et al. [24], since the electrical conductivity of a CNT-containing aerogel composite is continuously increased by increasing the amount of nanotubes (i.e. in Fig. 5), the percolation effect should be neglected and instead the effective medium theory (EMT) can be applied. As a result, the value of interfacial resistance, R_{σ}, calculated from EMT theory [21] was 1.46×10^{-11} and 1.93×10^{-11} Ωm^2 for CNT and CNF aerogel nanocomposites, respectively.

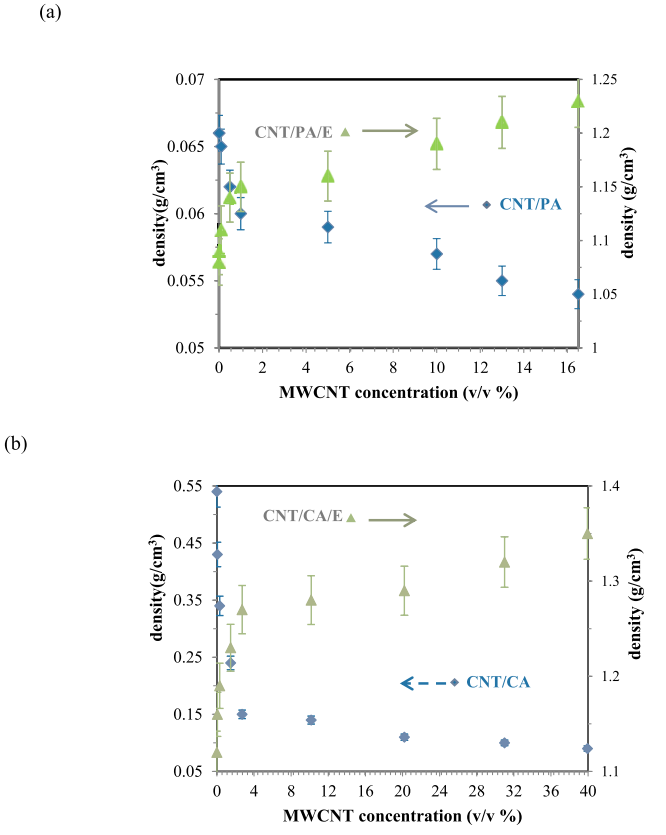

Fig. 4. Monolith density of aerogels and epoxy nanocomposites as a function of MWCNT concentration after (a) drying and (b) pyrolysis process.

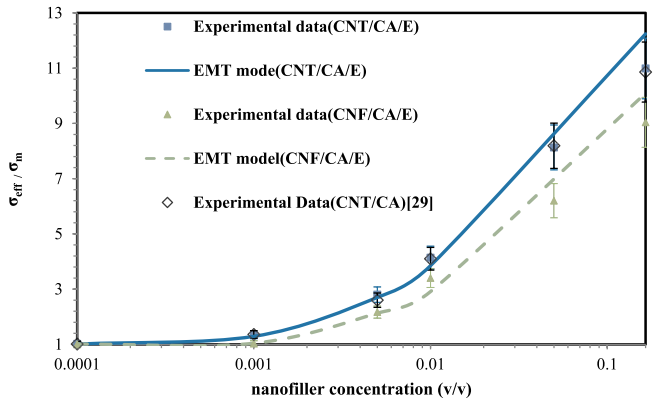

Fig. 5. Semi-log plot of relative electrical conductivity of the epoxy aerogel composites with respect to nanofiller volume fraction.

As one can observe, the interfacial resistance for CNT nanocomposite is lower than that of CNF ones. A better dispersion of CNT in resin can lead to a decrease in the interfacial resistance through the increase of the effective aspect ratio and thereby increase the formation of more perfect electrical current flow paths [25]. In order to investigate the effect of CNT content on electrical conductivity of epoxy matrixes, the electrical conductivity of CNT/PA/E and CNF/PA/E nanocomposites were drawn as a function of nanofiller content (Fig. 6). The σ_{eff} and σ_m were defined as the electrical conductivity of CNT/PA/E and the PA/E composite, respectively. It must be maintained that PAN aerogel is not conductive ($\sigma = 1.5 \times 10^{-11} Sm^{-1}$) [22]and also pure epoxy resin is insulator ($\sigma = \sim 10^{-12}$ Sm^{-1}) [23]. However, because of the large difference between the electrical conductivity of PA/E and CNT/PA/E composites, a sharp jump of about 4 orders of magnitude is observed in the curves at low nanotube concentration, exhibiting a percolation effect.

The electrical conductivity of the discontinuous phase in accordance with the percolation theory is obtained by the following equation:

$$\sigma \propto (\varnothing - \varnothing_c)^t \quad (2)$$

Where $\varnothing$ is the volume fraction of the discontinuous phase, $\varnothing_c$ is the volume fraction of percolation threshold, and t is the critical exponent, which is dependent on the dimensions of the system [23]. To determine $\varnothing_c$ and t, equation (2) was fitted to the experimental data. The amount of $\varnothing_c$ and t for epoxy nanocomposites were obtained and compared with the other research works in Table 3.

According to Haghgoo et al. [24], based on the excluded volume

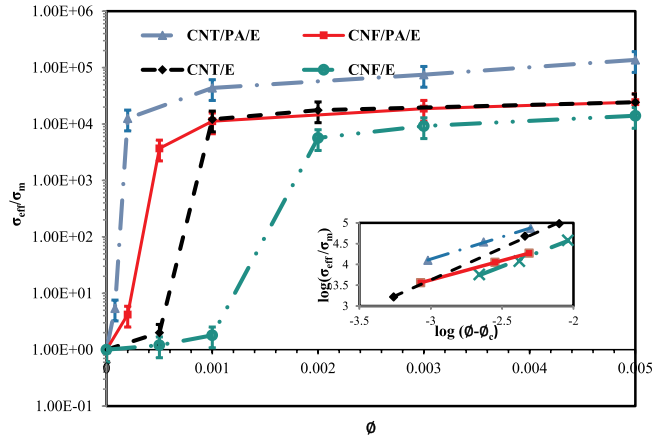

Fig. 6. Semi- log plot of the relative electrical conductivity of CNT and CNF containing epoxy with and without aerogel scaffold as a function of nanofiller volume fraction $\varnothing$: The insert shows a log–log plot of the conductivity as a function of ($\varnothing$ - $\varnothing_c$).

Table 3
Comparison of previous reports of the scaling law parameters with the present research work.

composite type	$\varnothing_c$ [a]	t	Reference
SWCNT/epoxy	5.2×10^{-5}	2.7	Bryning [39]
MWCNT/RF xerogel	2.5×10^{-4}	1.00	Haghgoo [31]
graphene aerogel/epoxy	6×10^{-4}	–	Jang-Kyo Kim [40]
MWCNT/epoxy	4×10^{-4}	2.28	Demont [41]
CNF/epoxy	3.2×10^{-4}	1.94	Hoa [42]
MWCNT/poly(ethylene terephthalate)	4.5×10^{-3}	2.2	Yang [40]
graphene-RF aerogel/epoxy	1.2×10^{-4}	–	Green [43]
SWCNT/epoxy	3.1×10^{-4}	2.68	Gao [44]
CNT/PA/E	2.8×10^{-5}	1.07	present work
CNT/E	4.5×10^{-4}	1.54	present work
CNF/PA/E	1.9×10^{-4}	1.33	present work
CNF/E	8.3×10^{-4}	1.96	present work

[a] Wherever the original data are given in wt.%, the conversion ratio of v % = 0.5 wt% is applied.

approach, an upper and a lower band can be obtained to the threshold for a randomly dispersed system of nanorods. The lower and upper limit are calculated directly from the length and outer diameter of the nanorods with and without the assumption of existing the interaction between the particles, respectively. Based on this theory, percolation threshold of CNTs in epoxy matrix is calculated as follows:

$$3.4 \times 10^{-4} < \varnothing_{c\_CNT} < 7.5 \times 10^{-3} \quad (3)$$

and for composites containing CNF, one can obtain:

$$7.26 \times 10^{-4} < \varnothing_{c\_CNF} < 1.1 \times 10^{-2} \quad (4)$$

As shown in Table 3, $\varnothing_c$ of the composites prepared by random mixing process (CNT/E and CNF/E) is in the range and quite close to the lower limits in eqs. (3) and (4).

However, for epoxy infiltrated aerogel nanocomposites, the experimental value of $\varnothing_c$ is far below the percolation theory range. Similar results were also reported by some authors [25]. Table 3 represents the comparison of the scaling law parameters in the published reports.

According to the obtained results, the CNT interconnected network structure markedly reduces the percolation thresholds of the epoxy composites. Here, aerogel is used as a nanofiller framework in resin matrix and its interconnected network is a key factor to achieve ultra-low percolation. This phenomena can be described by kinetic percolation [26], in which nanoparticles reaggregate during consolidation of their medium. The kinetic theory describes the percolation based on the free movement of particles within the matrix in concentrations of less than 0.1 wt% filler in nanocomposites. This theory is especially used to describe systems that exhibit low viscosity during the processing in which the motion of particles and creation of percolating paths can be controlled by shear forces, convection or external fields. This can develop filler-free micron-size parts of the matrix by lowering the fractal dimensionality of the system resulting in a drop of the percolation volume fraction. As shown in Table 3, the percolation threshold for CNT nanocomposite was lower than that of CNF nanocomposites. Similar results were reported by Al-Saleh [27]. At a certain value of nanofiller concentration, the tunneling distance between CNTs is lower than that between CNFs, bringing about a lower value of ∅c. Moreover, if t is taken into account as a measurement of system dimensionality [28], one can realize that the dimension of our nanocomposites is influenced by both the type of the nanofiller and the sample preparation method: dimensionality is lower in CNT-containing composites (than CNF) and the composites synthesized using infiltration method (compared to random mixing route).

3.3. Mechanical properties of aerogel nanocomposite

Impact of the MWCNT and CNF concentration on the Young's modulus of the nanocomposites is shown in Fig. 7. The compressive modulus of nanocomposite increases with nanofiller concentration. Results also show, in comparison with CNF nanocomposite, CNT/epoxy nanocomposites saw an increase in modulus and strength. The reason of this increase could be related to the higher aspect ratio and specific surface area of CNT-based ligaments. Epoxy composite with the CNT/PA scaffold (at 1 vol %) showed about 560% enhancement of Young's modulus (201 MPa) compared with the pure epoxy (30.5 MPa). This increase may be attributed to existence of an interconnected carbon nanotube network within the polymer matrix and its strong interface with the polymer matrix. Nanotubes with the high modulus and aspect ratio play an important role as a reinforcement filler to improve the mechanical properties of epoxy nanocomposites [29]. Nonetheless, surprisingly, CNT/E sample with the same amount of functionalized MWCNTs showed a 90% increase in compressive strength. These results showed that the nanocomposite containing prefabricated scaffolds are markedly superior to the conventional nanocomposites in mechanical properties. The agglomeration of CNT and CNF particles at high concentrations due to their poor dispersion in the matrix, and also their lower interfacial area compared to that of aerogels, leads to a reduction in the compressive modulus of the nanocomposites prepared by simple mixing.

To further utilize CNT and CNF aerogels in improving the mechanical properties of the composites, in the following, a comparison is made between theoretical models and empirical results. The Halpin–Tsai equation has been recognized for its ability to predict the modulus for the fiber reinforced composites [30]. The modified Halpin-Tsai model for MWCNT-reinforced matrix in a random direction is written as given below [31,32]:

$$E_{CNT} = \frac{3}{8}\frac{1 + 2\left\{\frac{L_{NT}}{d_{NT_0} - d_{NT_i}}\right\}\eta_L V_{NT}}{1 - \eta_L V_{NT}} + \frac{5}{8}\frac{1 + 2\eta_T V_{NT}}{1 - \eta_T V_{NT}} E_m \quad (7)$$

Where L_{NT} V_{NT}, d_{NT_0} and d_{NT_i} are the length, volume, outer and inner diameter of the MWCNTs .E_m is matrix Young's modulus and η_L and η_T take the following expressions:

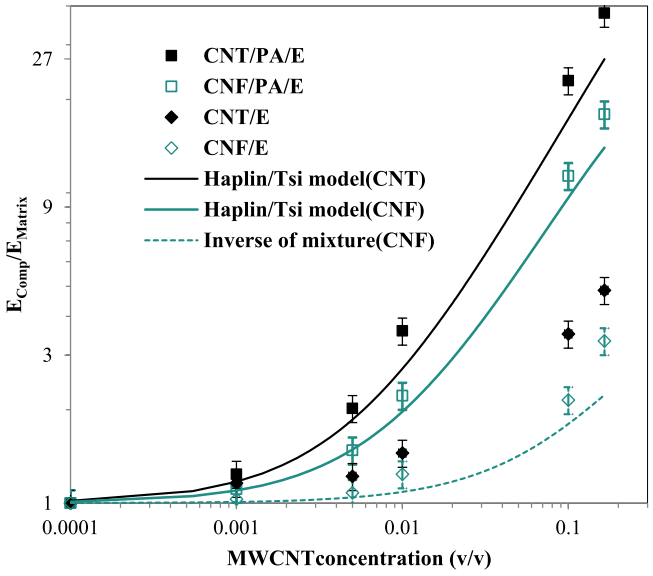

Fig. 7. Relative modules of the nanocomposites plotted versus volume fraction of nanofillers and comparison with Halpin-Tsai prediction.

$$\eta_L = \frac{\left(\alpha \frac{E_{NT}}{E_m}\right) - 1}{\alpha \frac{E_{NT}}{E_m} + 2\left(\frac{l_f}{Ed_f}\right)} \quad \text{and} \quad \eta_T = \frac{\left(\alpha \frac{E_f}{E_m}\right) - 1}{\alpha \frac{E_{NT}}{E_m} + 2} \tag{8}$$

In above equations, α is the direction factor and is equal to 1/6 for MWCNTs based nanocomposite [31]. As shown in Fig. 7, the elastic modulus increases with the increasing MWCNTs content. The modulus of CNT/PA/E nanocomposite is more consistent with the modified Halpin-Tasi model compared to the samples prepares by simple mixing. This can be attributed to the more homogeneous dispersion and stronger interface between CNTs and epoxy in CNT/PA/E specimens [7,33]. In these samples, CNT bundles are coated by a PAN shell; this brings about a strong bonding at the PAN-coated CNT/epoxy interface which is a major factor in the reinforcement of composites [15]. The results demonstrate the outstanding role of CNT aerogel scaffolding in improving the properties of nanocomposites. On the other hand, CNT/E samples show a good agreement with inverse rule of mixtures model which confirms the poor state of CNT dispersion throughout he mixture. This suggests that simple shear mixing cannot predominate the van der Waals attractions between the nanotubes. Another problem with simple shear mixing is the formation of voids during the process of mixing the hardener and the epoxy resin [34].

Regardless of nanocomposites' preparation method, samples containing CNTs showed higher elastic modulus in comparison with those prepared by CNFs. This suggests that aspect ratio of the nanofiller plays a key role in enhancement of mechanical properties of nanocomposites in both preparation routes.

3.4. Thermal properties of aerogel nanocomposite

TGA analysis is performed to evaluate the thermal stability of samples under air atmosphere (Fig. 8). All samples showed similar decomposition profiles with a two-stage degradation. The decomposition of pure epoxy started at 250 °C, whereas the composites started losing weight in the range of 280–295 °C and the residual char content of the resin decomposition can be measured. In composite materials, the percent residue at 700 °C is found to be higher than that obtained for pure epoxy matrix; in other words, the presence of the aerogel scaffold has led to a decrement in the mass loss caused by the degradation of the epoxy resin. Similar reports have been published by Oh et al. [35inpreparation] of polyurethane/CNT aerogel nanocomposite by backfilling the nanotube scaffolds as wet gels with polymer. Their report demonstrated that the formation of a thin layer from residues of polymer decomposition on the CNT network prevent nanotubes from destruction, up to a temperature of approximately 800 °C; While in the conventional composites, the protective layer does not form properly on the surface of large number of nanotubes [31]. The results show that by increasing the amount of nanofillers, polymer degradation is transferred to high temperature.

Improving temperature stability in the presence of MWCNTs and CNF can be due to the high thermal conductivity of these nanofillers that can increase the heat transfer path inside the composite and prevents the formation of hot spots within the composite, thereby preventing the thermal degradation. In addition, in aerogel nanocomposites, the pores of the CNT and CNF network may reduce polymer thermal motions; As a result of the molecular mobility of the trapped polymer chain in the aerogel network structure, the degradation of the polymer chains will also occur more slowly with increasing nanofiller content [35].

Fig. 9 displays the semi–log plot of the thermal conductivity of CNT and CNF nanocomposites as a function of nanofiller concentration. k_{eff} and k_m are the measured thermal conductivity of the nanocomposites and the pure epoxy, respectively. Not surprisingly, thermal conductivity of composites increased with the nanofiller content. As shown in Fig. 9, the thermal conductivity of nanocomposites underwent a continuous change with the increasing amount of nanofillers and thus no percolation effect was observed. The morphological differences between the composites prepared by mixing and infiltration method affect their thermal conductivity at a certain MWCNT loading. By forming a bicontinuous structure consisting of a rich nanotube network surrounded by epoxy resin, phonon transfer occurs in rich nanotube area [36]. The improvement in thermal conductivity of a CNT/PA/E sample with 1 v% MWNT is greater than that in a CNT/E sample with 16.5v% filler which contains discrete and agglomerated MWCNTs. By using EMT, interface thermal resistance between nanofiller and matrix, R_k was calculated for various nanocomposites according to Table 4 [37].

The obtained results showed that the CNT nanocomposites had higher k_{eff} and thus lower R_k than the CNFs. This is the result of two facts: a) more intrinsic thermal conductivity of individual nanotubes (3000 W/mk) than nanofibers (1800W/mk) [38] and b) better dispersion state of CNT than that of CNF throughout the matrix.

A three-dimensional interconnected network of nanotubes forms in aerogel nanocomposites which provides higher contact surface and resin matrix and suitable phonon transport. However, the development of nanofiber network structures is not possible due to further hardness and smaller aspect ratio.

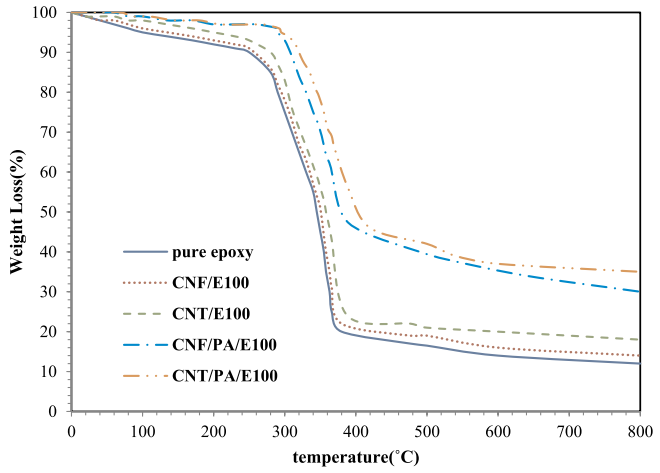

Fig. 8. TGA curves of epoxy/CNT and epoxy/CNF nanocomposites with and without aerogel scaffold under atmospheric air at 1 vol %.

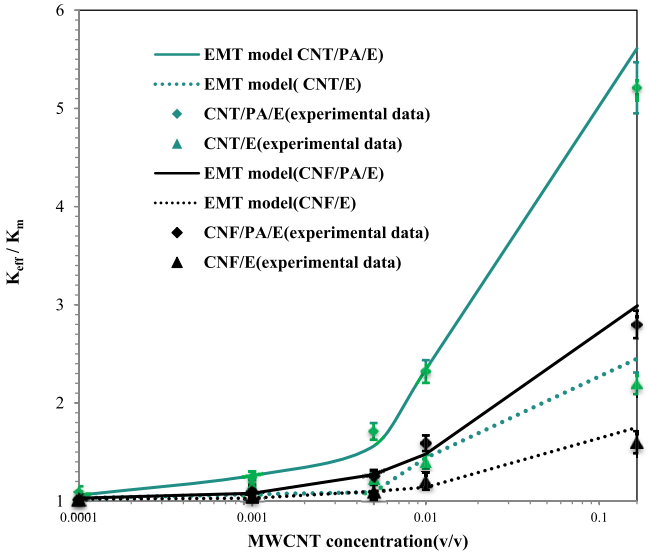

Fig. 9. Semi-log plot of the enhancement in thermal conductivity relative to pristine epoxy as a function of MWCNT and CNF concentration.

Table 4
The obtained results of R_k for CNT and CNF nanocomposites.

composite type	$R_k \times 10^{-8}$ (m^2KW^{-1})
CNT/PA/E	0.44
CNF/PA/E	0.84
CNT/E	3.6
CNF/E	7.9

4. Conclusions

In summary, novel CNT and CNF aerogel/epoxy nanocomposites were fabricated through infiltration of epoxy resin into the monolithic MWCNT (or CNF)/PAN aerogel framework. The formation of a three dimensional CNT and CNF network was carried out using TIPS method. Physical and transport properties of nanocomposites were measured and compared with the sample prepared by simple mixing method.

The corresponding structure showed greatly enhanced strength in compression modulus according to Halpin-Tsai model. The composite also demonstrated an ultra-low electrical percolation threshold and much improved thermal conductivity (680% at 16.5% CNT relative to pure epoxy). These were attributed to the bicontinuous morphology of the nanocomposites prepared by infiltration method.

Better dispersion and orientation of the nanofiller at low concentration in three dimensional networks, are characteristic of infiltration method which can be applied to produce high performance composites.

The exceptional properties of theses composites provides a capacity to utilize a new class of nanocomposites based on aerogel scaffolds, which can have wide applications in the field of high efficiency and multi-functional materials for use in aerospace and automobile applications and devices such as sensors, electrodes and actuators.

References

[1] Aradhana R, Mohanty S, Nayak SK. High performance epoxy nanocomposite adhesive: effect of nanofillers on adhesive strength, curing and degradation kinetics. Int J Adhesion Adhes 2018;84:238–49. https://doi.org/10.1016/j.ijadhadh.2018.03.013.

[2] Wang Y, Chen S, Chen X, Lu Y, Miao M, Zhang D. Controllability of epoxy equivalent weight and performance of hyperbranched epoxy resins. Compos Part B 2019;160:615–25. https://doi.org/10.1016/j.compositesb.2018.12.103.

[3] Liu S, Chevali VS, Xu Z, Hui D, Wang H. A review of extending performance of epoxy resins using carbon nanomaterials. Compos Part B 2017. https://doi.org/10.1016/j.compositesb .2017.08.020.

[4] Bordjiba T, Mohamedi M, Dao LH. New class of carbon-nanotube aerogel electrodes for electrochemical power sources. Adv Mater 2008;20:815–9. https://doi.org/10.1002/adma.200701498.

[5] Su H, Jang J, Yu J, Yun S. Thermal conductivity of polymer composites based on the length of multi-walled carbon nanotubes, vol. 79; 2015. p. 505–12. https://doi.org/10.1016/j.compositesb .2015 .05 .012.

[6] Li S, Yao Y. Synergistic improvement of epoxy composites with multi-walled carbon nanotubes and hyperbranched polymers. Compos Part B 2018. https://doi.org/10.1016/j.compositesb .2018.11.122.

[7] Zou J, Liu J, Karakoti AS, Kumar A, Joung D, Li Q, et al. Ultralight multiwalled carbon nanotube aerogel. ACS Nano 2010;4:7293–302. https://doi.org/10.1021/nn102246a.

[8] Haghgoo M, Plougonven E, Yousefi AA, Pirard JP, Léonard A, Job N. Use of X-ray microtomography to study the homogeneity of carbon nanotube aqueous suspensions and carbon nanotube/polymer composites. Carbon N Y 2012;50:1703–6. https://doi.org/10.1016/j.carbon .2011.11.031.

[9] Zhang D, Villarreal MG, Cabrera E, Benatar A, Lee LJ, Castro JM. Performance study of ultrasonic assisted processing of. Compos Part B 2018. https://doi.org/10.1016/j.compositesb .2018. 10.012.

[10] Kim MT, Rhee KY, Park SJ, Hui D. Composites : Part B Effects of silane-modified carbon nanotubes on flexural and fracture behaviors of carbon nanotube-modified epoxy/basalt composites, vol. 43; 2012. p. 2298–302. https://doi.org/10.1016/j.compositesb.2011.12.007.

[11] Lin Z, Zeng Z, Gui X, Tang Z, Zou M, Cao A. Carbon nanotube sponges, aerogels, and hierarchical composites: synthesis, properties, and energy applications. Adv Energy Mater 2016;6. https://doi.org/10.1002/aenm.201600554.

[12] Zhao W, Li Y, Wu S, Wang D, Zhao X, Xu F, et al. Highly stable carbon nanotube/polyaniline porous network for multifunctional applications. ACS Appl Mater Interfaces 2016;8:34027–33. https://doi.org/10.1021/acsami.6b11984.

[13] Bryning MB, Milkie DE, Islam MF, Hough LA, Kikkawa JM, Yodh AG. Carbon nanotube aerogels. Adv Mater 2007;19:661–4. https://doi.org/10.1002/adma.200601748.

[14] Hajian A, Fu Q, Berglund LA. Recyclable and superelastic aerogels based on carbon nanotubes and carboxymethyl cellulose. Compos Sci Technol 2018;159:1–10. https://doi.org/10.1016/j.compscitech.2018.01.002.

[15] Worsley MA, Kucheyev SO, Kuntz JD, Olson TY, Han TYJ, Hamza AV, et al. Carbon scaffolds for stiff and highly conductive monolithic oxide-carbon nanotube composites. Chem Mater 2011;23:3054–61. https://doi.org/10.1021/cm200426k.

[16] Gui X, Li H, Zhang L, Jia Y, Liu L, Cao A. A facile route to isotropic conductive nanocomposites by direct polymer in fi ltration of carbon nanotube. 2011. p. 4276–83.

[17] Hu H, Zhao Z, Wan W, Gogotsi Y, Qiu J. Polymer/graphene hybrid aerogel with high compressibility, conductivity, and " sticky " superhydrophobicity. 2014.

[18] Wang Z, Shen X, Akbari Garakani M, Lin X, Wu Y, Liu X, et al. Graphene aerogel/epoxy composites with exceptional anisotropic structure and properties. ACS Appl Mater Interfaces 2015;7:5538–49. https://doi.org/10.1021/acsami.5b00146.

[19] Dourani A, Hamadanian M, Haghgoo M, Jahannama MR, Goudarzi H. Morphology and electrical properties of multi-walled carbon nanotube/carbon aerogel prepared by using polyacrylonitrile as precursor. RSC Adv 2015;5:49944–52.

[20] Dourani A, Haghgoo M, Hamadanian M, Mehdinavaz R. Effect of carbon nanotube loading on mechanical and thermal properties of pure and pyrolyzed. J Nanosci Nanotechnol 2017;17. https://doi.org/10.1166/jnn.2017.13068.

[21] Dante RC. Handbook of friction materials and their applications. Handb Frict Mater Their Appl 2016:29–54. https://doi.org/10.1016/B978-0-08-100619-1.00003-1.

[22] Ahmad A, Isa KBM, Osman Z. Conductivity and structural studies of plasticized polyacrylonitrile (PAN)-lithium triflate polymer electrolyte films. Sains Malays 2011;40:691–4.

[23] Khan SU, Pothnis JR, Kim JK. Effects of carbon nanotube alignment on electrical and mechanical properties of epoxy nanocomposites. Compos Part A Appl Sci Manuf 2013;49:26–34. https://doi.org/10.1016/j.compositesa.2013.01.015.

[24] Haghgoo M, Yousefi AA, Zohouriaan Mehr MJ, Celzard A, Fierro V, Léonard A, et al. Characterization of multi-walled carbon nanotube dispersion in resorcinol-formaldehyde aerogels. Microporous Mesoporous Mater 2014;184:97–104. https://doi.org/10.1016/j.micromeso. 2013.10.002.

[25] Haghgoo M, Yousefi AA, Mehr MJZ, Léonard FA, Philippe MP, et al. Correlation between morphology and electrical conductivity of dried and carbonized multi-walled carbon nanotube/resorcinol???formaldehyde xerogel composites. J Mater Sci 2015;50:6007–20. https://doi.org/10.1007/s10853-015-9148-0.

[26] Bauhofer W, Kovacs JZ, Swan T, Swan T, Swan T. A review and analysis of electrical percolation in carbon nanotube polymer composites. Compos Sci Technol 2009;69:1486–98. https://doi.org/10.1016/j.compscitech.2008.06.018.

[27] Al-Saleh MH, Saadeh WH, Sundararaj U. EMI shielding effectiveness of carbon based nanostructured polymeric materials: a comparative study. Carbon N Y 2013;60:146–56. https://doi.org/10.1016/j.carbon.2013.04.008.

[28] Kohlmeyer RR, Lor M, Deng J, Liu H, Chen J. Preparation of stable carbon nanotube aerogels with high electrical conductivity and porosity. Carbon N Y 2011;49:2352–61. https://doi.org/10.1016/j.carbon.2011.02.001.

[29] Gantayat S, Rout D, Swain SK. Carbon nanomaterial–reinforced epoxy composites: a review. Polym Plast Technol Eng 2018;57:1–16. https://doi.org/10.1080/03602559.2017.1298802.

[30] Srivastava VK. Modeling and mechanical performance of carbon nanotube/epoxy resin composites. Mater Des 2012;39:432–6. https://doi.org/10.1016/j.matdes.2012.02.039.

[31] Srivastava V K, Singh S. A micro-mechanical model for elastic modulus of multi-walled carbon nanotube/epoxy resin composites. Int J Compos Mater 2012;2:1–6. https://doi.org/10.5923/j.cmaterials.20120202.01.

[32] Kim M, Mirza FA, Song JI. Micromechanics modeling for the stiffness and strength properties of glass fibers/CNTs/epoxy composites. WIT Trans Built Environ 2010;112:279–90. https://doi.org/10.2495/HPSM100261.

[33] Worsley MA, Pauzauskie PJ, Kucheyev SO, Zaug JM, Hamza AV, Satcher JH, et al. Properties of single-walled carbon nanotube-based aerogels as a function of nanotube loading. Acta Mater 2009;57:5131–6. https://doi.org/10.1016/j.actamat.2009.07.012.

[34] Liu J, Chen C, Feng Y, Liao Y, Ye Y, Xie X, et al. Ultralow-carbon nanotube-toughened epoxy: the critical role of a double-layer interface. ACS Appl Mater Interfaces 2018;10:1204–16. https://doi.org/10.1021/acsami.7b14767.

[35] Oh Y, Islam MF. Preformed nanoporous carbon nanotube sca ff old-based. 2015. https://doi.org/10.1021/acsnano.5b00170. 4103–10.

[36] Kashiwagi T, Du F, Douglas JF, Winey KI, Harris RH, Shields JR. Nanoparticle networks reduce the flammability of polymer nanocomposites. Nat Mater 2005;4:928–33. https://doi.org/10.1038/nmat1502.

[37] Mateusz B. Bryning. Carbon nanotube networks in epoxy composites and aerogels. 2007.

[38] Gardea F, Naraghi M, Lagoudas D. Effect of thermal interface on heat flow in carbon nanofiber composites. Appl Mater Interfaces 2014;6:1061–72.

[39] Bryning MB, Islam MF, Kikkawa JM, Yodh AG. Very low conductivity threshold in bulk isotropic single-walled carbon nanotube-epoxy composites. Adv Mater 2005;17:1186–91. https://doi.org/10.1002/adma.200401649.

[40] Li J, Ma PC, Chow WS, To CK, Tang BZ, Kim JK. Correlations between percolation threshold, dispersion state, and aspect ratio of carbon nanotubes. Adv Funct Mater 2007;17:3207–15. https://doi.org/10.1002/adfm.200700065.

[41] Barrau S, Demont P, Maraval C, Bernes A, Lacabanne C. Glass transition temperature depression at the percolation threshold in carbon nanotube-epoxy resin and polypyrrole-epoxy resin composites. Macromol Rapid Commun 2005;26:390–4. https://doi.org/10.1002/marc.200400515.

[42] Allaoui A, Hoa SV, Pugh MD. The electronic transport properties and microstructure of carbon nanofiber/epoxy composites. Compos Sci Technol 2008; 68:410–6. https://doi.org/10.1016/j.compscitech.2007.06.028.
[43] Irin F, Das S, Atore FO, Green MJ. Ultralow percolation threshold in aerogel and cryogel templated composites. Langmuir 2013;29:11449–56. https://doi.org/10.1021/la4017307.
[44] Li N, Huang Y, Du F, He X, Lin X, Gao H. Electromagnetic interference (EMI) shielding of single-walled carbon nanotube epoxy composites. Nano Lett 2006;6: 1–5.